Grignard Reagents in Solution: Theoretical Study of the Equilibria and the Reaction with a Carbonyl Compound in Diethyl Ether Solvent

Toshifumi Mori and Shigeki Kato*

Department of Chemistry, Graduate School of Science, Kyoto University, Kitashirakawa, Sakyo-ku, Kyoto 606-8502, Japan

Received: February 3, 2009; Revised Manuscript Received: March 15, 2009

The equilibria of Grignard reagents, CH_3MgCl and CH_3MgBr, in diethyl ether (Et_2O) solvent as well as the reaction of the reagents with acetone are studied theoretically. To describe the equilibria and reactions in Et_2O solvent, we employ the reference interaction site model self-consistent field method with the second-order Møller−Plesset perturbation (RISM-MP2) free energy gradient method. Since the solvent molecules strongly coordinate to the Grignard reagents, we construct a cluster model by including several Et_2O molecules into the quantum mechanical region and embed it into the bulk solvent. We propose that, instead of the traditionally accepted cyclic dimer, the linear form of dimer is as stable as the monomer pair and participates in the equilibria. For the reaction with acetone, two important reaction paths (i.e., monomeric and linear dimeric paths) are studied. It is found that the barrier height for the monomeric path is much higher than that for the linear dimeric path, indicating that the reaction of the Grignard reagent with acetone proceeds through the linear dimeric reaction path. The change of solvation structure during the reaction is examined. On the basis of the calculated free energy profiles, the entire reaction mechanisms of the Grignard reagents with aliphatic ketones in Et_2O solvent are discussed.

1. Introduction

Grignard reagents, the organometallics that react with carbonyl or allyl compounds and form C−C bonds in the products, have been utilized in organic synthesis for more than 100 years.[1−3] Because of the importance and usefulness of Grignard reagents in various applications, the reaction mechanisms have been continuously studied. For example, the stereoselective addition of Grignard reagents to carbonyl compounds has been a topic of experimental[4,5] and theoretical[6,7] studies in recent years. Despite these activities in studying the Grignard reactions, details of the reaction mechanisms are still vague, particularly for the role of solvents, which is important in characterizing the reaction mechanisms.

The Grignard reagents are formally written as RMgX, where R is an alkyl group and X is a halide. However, their actual structures in solution are far more complicated. Traditionally, they have been expressed in the form of the equilibria

$$(RMgX)_2 \rightleftharpoons 2RMgX \rightleftharpoons R_2Mg + MgX_2 \qquad (1)$$

Here, the former is known as the dimerization equilibrium, whereas the latter is the Schlenk one. Crystallographic studies on the solvated structures of the species in eq 1 have been performed,[8,9] and they found that the Mg atoms in Grignard reagents are stable in tetrahedrally coordinated form. Experimental studies on eq 1 have also been performed by calorimetric,[10−12] molecular weight,[13,14] and ebullioscopic measurements[15] as well as NMR spectroscopy.[16] These suggested that the dimerization equilibrium is dominant in diethyl ether (Et_2O) solvent, though the Schlenk equilibrium is preferable in tetrahydrofuran (THF). It was also found that alkylmagnesium bromides (RMgBr) in Et_2O solvent are monomeric at low concentration (<0.1 M) and are dimeric at higher concentrations (>0.5 M), whereas alkylmagnesium chlorides (RMgCl) are dimeric even at low concentration.[1,2,13,15,17]

Theoretical studies on Grignard reagents have been carried out by ab initio methods[18] and density functional theory (DFT),[19−21] as well as semiempirical calculations.[22,23] From these studies, the binding energies of solvent molecules to Mg atoms in Grignard reagents were found to be very large and also quite sensitive to the level of computational methods. For example, the binding energy of two dimethyl ether (Me_2O) molecules to CH_3MgCl was 28.4 kcal/mol by DFT method,[20] whereas it became 46.8 kcal/mol by the second-order Møller−Plesset perturbation (MP2) method.[18] The dimerization energy was also sensitive to the methods.[18,21] On the other hand, the Schlenk equilibrium was well described by both DFT and MP2 methods (i.e., the energy difference between $2CH_3MgCl\cdot(Me_2O)_2$ and $(CH_3)_2Mg\cdot(Me_2O)_2 + MgCl_2\cdot(Me_2O)_2$ was 3.1−3.6 kcal/mol at DFT or MP2 level).[18,20]

Grignard reactions usually proceed in solvents such as Et_2O and THF. The solvent effects on the reaction mechanisms have been studied with the continuum solvent models.[6,7] However, since solvent molecules strongly coordinate to Grignard reagents, more elaborate models reflecting molecular aspects of solvent may be required to describe the solvation effects. Recently, we developed the analytic free energy gradient for the reference interaction site model self-consistent field (RISM-SCF) method with the MP2 energy (i.e., RISM-MP2 free energy gradient method).[24] This method was applied to study the equilibria of CH_3MgCl in Me_2O solvent. We found that the effect of dynamic electron correlation as well as that of bulk solvent were important for describing the dimerization and Schlenk equilibria.

In the present article, we study the reaction of Grignard reagent CH_3MgCl with acetone in Et_2O solvent. Since Et_2O is one of the most common solvents in organic synthesis studies, we employ this solvent instead of Me_2O. Note that the boiling

* To whom correspondence should be addressed. E-mail: shigeki@kuchem.kyoto-u.ac.jp.

10.1021/jp9009788 CCC: $40.75
Published on Web 05/06/2009

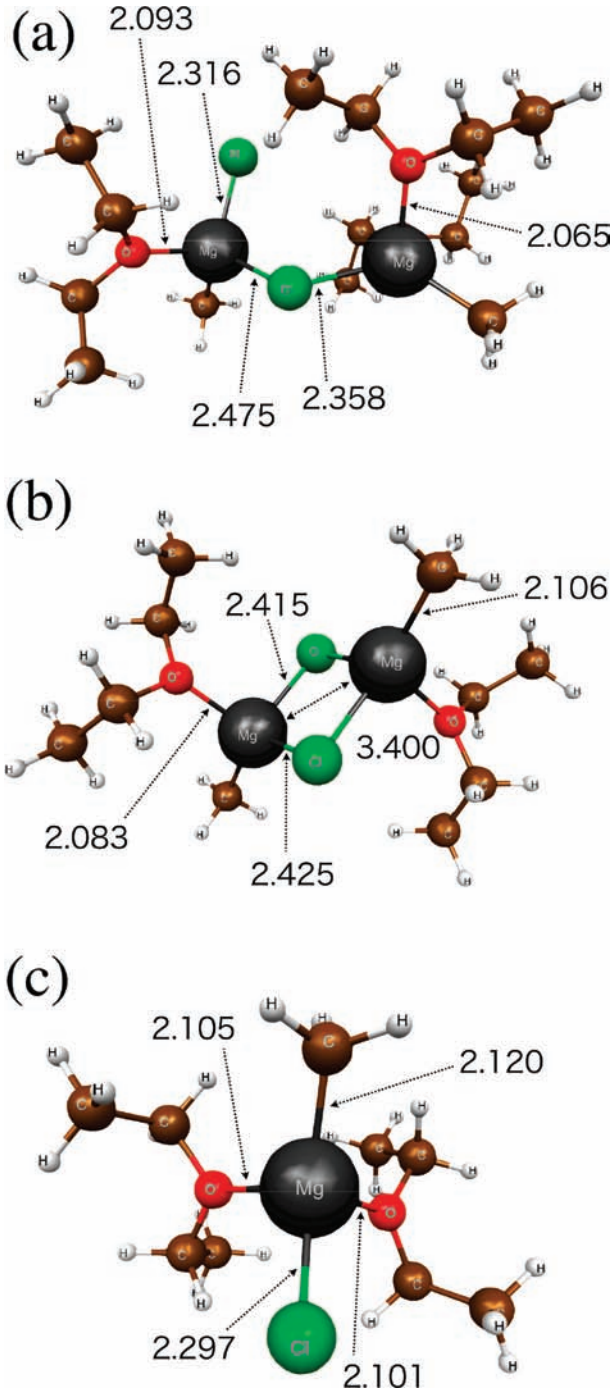

Figure 1. Equilibrium geometries of (a) linear dimer, (b) cyclic dimer, and (c) monomer, obtained by RISM-MP2 method. Distances are in angstroms.

point of Et_2O, 307.8 K, is much higher than that of Me_2O, 248.2 K. The purpose of the present work is twofold. One is to obtain a satisfactory explanation of the equilibria of Grignard reagents in Et_2O solvent. We calculate the solvation free energies of monomeric and dimeric forms of the reagents. For the dimer, we propose a new linear form as shown in Figure 1a, which is more stable than the traditional cyclic dimer in Figure 1b. The other is to clarify the mechanism of reaction in solution. We carry out calculations on the reactions of monomeric and dimeric forms of the reagent with acetone. To see the role of halide in Grignard reactions, we further study the equilibria and reaction for CH_3MgBr reagent, and the results are compared with those for CH_3MgCl.

2. Computational Details

In the RISM-MP2 method,[24] the free energy for a closed shell molecule is given by

$$F^{\mathrm{MP2}} = E_{\mathrm{solute}}{}^{\mathrm{HF}} + \Delta\mu + E^{(2)}$$
$$= \langle \Psi_{\mathrm{HF}} | \hat{H}_{\mathrm{gas}} | \Psi_{\mathrm{HF}} \rangle + \Delta\mu + \frac{1}{4}\sum_{i,j}^{\mathrm{occ}} \sum_{a,b}^{\mathrm{vir}} (ij|ab) \frac{2(ij|ab) - (ib|aj)}{\varepsilon_i + \varepsilon_j - \varepsilon_a - \varepsilon_b} \quad (2)$$

where the suffixes i,j and a,b denote the occupied and virtual orbitals, respectively. $\hat{H}_{\mathrm{gas}}$ is the solute Hamiltonian in gas phase, and $\Delta\mu$ is the excess chemical potential that is calculated with the correlation functions obtained by solving the RISM integral equations.[25,26] Ψ_{HF} is the solute Hartree−Fock (HF) wave function composed of the orbitals obtained by solving the solvated Fock equation derived from the Hamiltonian

$$\hat{H} = \hat{H}_{\mathrm{gas}} + \sum_{\alpha}^{\mathrm{site}} \hat{Q}_\alpha V_\alpha \quad (3)$$

Here, $\hat{Q}_\alpha$ is the population operator generating the partial charge Q_α on the solute site α, and V_α is the electrostatic potential acting on the same site, respectively. The orbital energy ε_i (in eq 2) is given as an eigenvalue of the solvated Fock operator including the solvation effect. The equilibrium geometries were obtained using the analytical gradients of the free energy,[24] and the vibrational frequencies were calculated by numerically differentiating the free energy gradients. The zero point energy (ZPE) corrections were also evaluated from these vibrational frequencies and are included in all the energies throughout the present article unless otherwise mentioned.

The effective core potential with the (5s,5p,1d)/[2s,2p,1d] basis set proposed by Stevens et al.[27] was employed for Br. For the other atoms, the 6-31G** basis set was employed. The effective charges on solute sites, Q_α, were determined by the restrained electrostatic potential method[28] with the grid points generated by the Spackman procedure.[29]

The coordination of solvent Et_2O molecules to Mg atoms in Grignard reagents is known to be quite important.[18−20,24] In the framework of the RISM-SCF method, the charges on solute sites (atoms) and distribution of solvent around these sites are determined self-consistently by coupling quantum mechanical calculations and statistical RISM integral equation of solvent.[25,26] Here, the interaction between solute and solvent is described by the site−site electrostatic and Lennard-Jones (LJ) potentials. However, since the strong dative bonding effects cannot be described sufficiently by the sum of these potentials, we introduced several Et_2O molecules into the quantum mechanical (QM) region to take into account the strong coordination effects. Since the experiments show that a Mg atom is coordinated to be a tetrahedral structure, we included Et_2O molecules in the QM region so that Mg atoms are tetrahedrally coordinated.

The effect of bulk Et_2O solvent was treated through the RISM integral equation coupled with the hypernetted chain closure relation. The potential parameters of solvent Et_2O molecule and LJ parameters of solute molecules were taken from the literature[24,30−33] and are given in Supporting Information. The temperature and density of solvent were fixed to 298.0 K and 5.75×10^{-3} molecule/Å^3, respectively.

We employed the united-atom model for Et_2O molecules in bulk solvent, and thus each solvent molecule consists of five sites (i.e., O, two CH_2, and two CH_3 groups). It is known that an Et_2O molecule can take the trans and gauche conformations where the $CH_3-CH_2-O-CH_3$ dihedral angles are different.

According to the Monte Carlo simulation calculations by Briggs et al.,[30] liquid Et_2O consists of mainly the trans−trans (tt) conformer (70%), with the trans−gauche (tg) (26%) and two gauche−gauche ($g^+ g^+$, $g^+ g^-$) isomers (1%, 2%). We therefore assumed that the bulk Et_2O solvent molecules take the tt structure for convenience. It is noted that we also carried out calculations with the solvent molecules fixed to the tg conformation, but the difference in solvation free energy of CH_3MgCl was within 1.0 kcal/mol between the tt and tg cases.

Et_2O molecules in the QM region were also treated by the united-atom model in solving the RISM equation, and the details are given in Appendix. We emphasize here that no geometric constraint was applied to Et_2O molecules in the QM region. Indeed, as seen in the next section, the geometries of Et_2O molecules in the QM region were close to the $g^+ g^-$ conformer, because of the steric effects between the Grignard reagent and coordinated Et_2O molecules.

To examine the effect of bulk solvent, we also carried out calculations for the Grignard reagents without the bulk solvent. Note that, even in this case, the strongly coordinating Et_2O molecules were included in the QM region. All the calculations were performed by the GAMESS quantum chemistry package,[34] in which we implemented our own RISM-MP2 routine.

3. Results and Discussion

3.1. Equilibria. We discuss here the equilibria of the Grignard reagents CH_3MgCl and CH_3MgBr in Et_2O solvent. Since the solvent Et_2O molecules, which strongly coordinate to Mg atoms to be a tetrahedral form, are treated quantum mechanically, we rewrite eq 1 in the following form:

$$\begin{aligned}&(CH_3MgX)_2\cdot(Et_2O)_2 + 2Et_2O\ (I)\\ \rightleftharpoons&(CH_3MgX)_2\cdot(Et_2O)_3 + Et_2O\ (II)\\ \rightleftharpoons&2CH_3MgX\cdot(Et_2O)_2\ (III)\\ \rightleftharpoons&(CH_3)_2Mg\cdot(Et_2O)_2 + MgX_2\cdot(Et_2O)_2\ (IV)\end{aligned} \qquad (4)$$

where X is Cl or Br. For the dimerization equilibrium, we considered the linear dimer (II) in addition to the traditional cyclic dimer (I). Since the Mg atom is tetrahedrally coordinated in each species in the equilibria (eq 4), the linear dimer is formed from two monomers by replacing one Et_2O molecule coordinated to one of the monomers with the halogen atom of the other monomer ((III) ⇌ (II)). The cyclic dimer (I) is further produced from the linear dimer (II) by eliminating one Et_2O and forming a new Mg−X dative bond. Note that the dimerization equilibrium, (III) ⇌ (II) ⇌ (I), is expected to be achieved easily because the substitution reaction of reagents at the Mg center is considered to be a very fast process.[1,16,17,19] Since the number of Et_2O molecules in the QM region is four for the species (III) and (IV), we regarded the extra Et_2O molecules in (I) and (II) as the solute molecules solvated in the bulk solvent. Thus, the number of Et_2O molecules in the QM region is conserved in each step included in eq 4.

The geometries optimized by RISM-MP2 method are shown in Figure 1, and the energies of the equilibria (eq 1) are given in Figure 2 and Table 1. The Schlenk equilibrium (III) ⇌ (IV) of CH_3MgCl was calculated to be endothermic by 3.4 kcal/mol with the RISM-MP2 method. The endothermicity was increased to 4.4 kcal/mol when substituting Br for Cl, as seen in Figure 2. These results are consistent with previous calculations.[19,21]

The energy of CH_3MgCl cyclic dimer (I) is higher than that of the monomer pair (III) by 4.7 kcal/mol in Et_2O solvent. For CH_3MgBr, the cyclic dimer becomes more unstable (i.e., 11.0 kcal/mol higher than the monomer pair). Thus, the cyclic dimer is not likely to be formed in Et_2O solvent from the present calculations. On the other hand, the energy of CH_3MgCl linear dimer (II) is very close to that of the monomer pair (III), as seen in Figure 2. The formation of linear dimer from the monomer pair ((III) ⇌ (II)) was endothermic by only 0.9 kcal/mol in Et_2O solvent. By substituting Br for Cl, the endothermicity increased to 3.6 kcal/mol. Therefore, the present calculations indicate that the dimer of Grignard reagents is considered to be of a linear form, not a cyclic one, because the formation of a cyclic dimer from a linear one is a very endothermic process with energy of 3.8 and 7.4 kcal/mol for CH_3MgCl and CH_3MgBr, respectively.

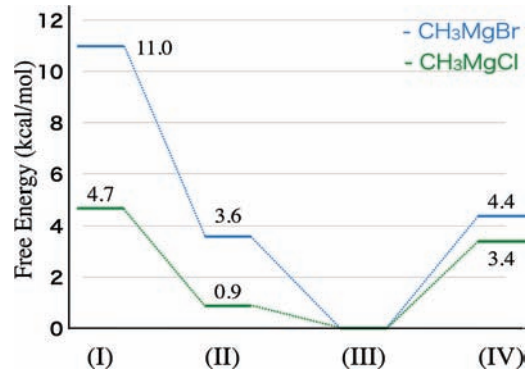

Figure 2. Energies of the species in the equilibria. Blue and green lines are for CH_3MgBr and CH_3MgCl, respectively. Energy of the monomer pair is set to zero.

TABLE 1: Change in Energies Due to Dimer Formations and Its Components (in Kilocalories per Mole)[a]

	ΔE (total)	ΔE_{solute}^{HF}	$\Delta\Delta\mu$	$\Delta E^{(2)}$	ΔE (ZPE)
CH_3MgCl					
linear dimer (II)	0.9 (−3.6)	1.2 (0.7)	4.9	−4.5 (−3.5)	−0.7 (−0.8)
cyclic dimer (I)	4.7 (3.7)	0.4 (0.7)	1.7	4.8 (5.2)	−2.2 (−2.2)
CH_3MgBr					
linear dimer (II)	3.6 (−0.5)	2.8 (3.6)	3.7	−1.7 (−3.4)	−1.2 (−0.7)
cyclic dimer (I)	11.0 (9.7)	4.1 (4.8)	2.2	6.9 (7.1)	−2.2 (−2.2)

[a] The energy of the monomer pair is set to zero. Values in parentheses are energies without bulk solvent.

To see the effect of bulk Et_2O solvent on the dimerization equilibrium, we obtained the geometries and energies of the species in the equilibria (eq 4) without the bulk solvent. The resultant energies are given in Table 1. In contrast to the case in solution, the formation of linear dimer became exothermic by 3.6 and 0.5 kcal/mol for CH_3MgCl and CH_3MgBr, respectively, without the bulk solvent. The energy difference between the cyclic dimer and the monomer pair was reduced to be 3.7 and 9.7 kcal/mol for the Cl and Br compounds.

Figure 3 shows the radial distribution functions (RDFs) between O atom in the bulk solvent and Mg atom in CH_3MgCl for the monomer, linear dimer, and cyclic one. We can find mainly two peaks at the distances of about 3 and 7−8 Å for all RDFs. The coordination numbers of bulk Et_2O molecules, obtained by integrating the first peaks of RDFs, were 0.31 for the monomer, 0.45 and 0.19 for the linear dimer, and 0.27 and 0.27 for the cyclic dimer, respectively. This indicates that there can exist the species in which a Mg atom is pentagonally coordinated in Et_2O solvent, though their populations are small because the coordination numbers are much smaller than 1.0. Thus, the first solvation shell of Mg atom is considered to be almost saturated by the Et_2O molecules in the QM region.

In a previous article, the cyclic dimer of CH_3MgCl in Me_2O solvent was studied.[24] The coordination number of the bulk

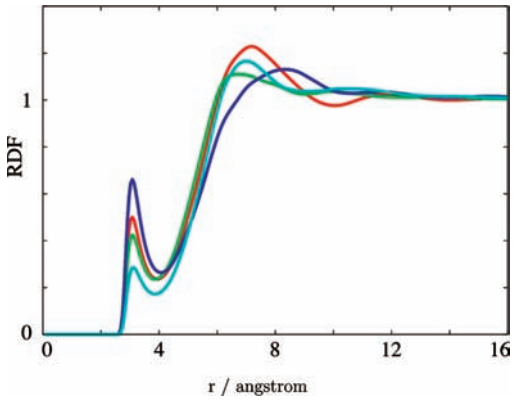

Figure 3. Radial distribution functions between Mg in Grignard reagent CH_3MgCl and O in Et_2O. Red, blue, and green lines are for monomer, linear dimer (dark: Mg1, light: Mg2), and cyclic dimer.

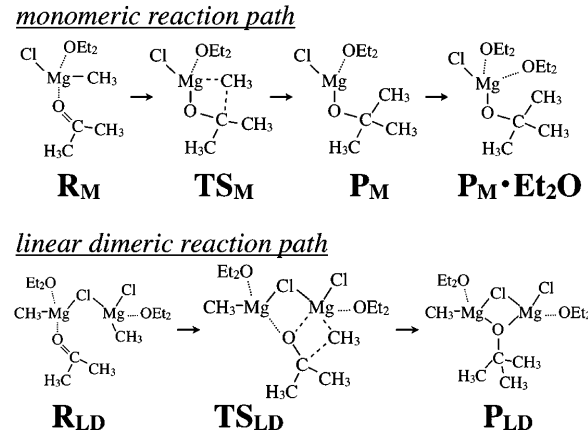

Figure 4. Scheme of the monomeric and linear dimeric reactions.

Me_2O solvent in the first solvation shell was larger than the present Et_2O value. This result is consistent with the weaker effect of bulk Et_2O solvent than Me_2O. Actually, the energy of cyclic dimer in Me_2O was higher than the monomer pair by 12.4 kcal/mol without ZPE correction, which is larger than the corresponding energy in Et_2O solvent, 6.9 kcal/mol.

Experimentally, the free energy change for the Schlenk equilibrium in Et_2O solvent was measured for CH_3MgBr, 3.4 kcal/mol,[12] which is comparable with the present result, 4.4 kcal/mol. For the dimerization equilibrium, experiments suggested that CH_3MgBr in Et_2O solvent is monomeric at low concentration, whereas CH_3MgCl in Et_2O solvent is dimeric even at low concentration.[13,15,17] As mentioned above, the traditional cyclic dimer is not likely to participate in the equilibrium, and the dimer observed in the experiments is considered to be of a linear form. Although the formation of linear dimer was calculated to be slightly endothermic for both CH_3MgCl and CH_3MgBr, the endothermicity is mainly attributed to a relatively large positive value for the change of excess chemical potential ($\Delta\Delta\mu$), 4.9 and 3.7 kcal/mol for CH_3MgCl and CH_3MgBr, respectively (Table 1). Since the RISM theory has a trend to overestimate the component of cavity formation energy in estimating the excess chemical potential,[35] the present values for $\Delta\Delta\mu$ might be too large. Taking account of this fact, the present results for the linear dimers are consistent with the experimental findings.

3.2. Reaction with Acetone. We now examine the reaction mechanism of the Grignard reagent CH_3MgCl with acetone in Et_2O solvent, particularly the reactions of the monomer and linear dimer, since these are dominant in Et_2O solvent, as shown above. The reaction path of the cyclic dimer was also calculated for comparison.

To initiate the reactions, one of the coordinated Et_2O molecules needs to be replaced by an acetone molecule, resulting in a complex of Grignard reagent with acetone. Note that this complexation process is observed to occur rapidly in the experiments.[1,17] After the Grignard reagent−acetone complex is produced, the C−C bond formation reaction occurs. The reaction schemes for the monomer and linear dimer complexes are depicted in Figure 4.

The substitution reaction of acetone for Et_2O is expressed as

$$Z\cdot(Et_2O)_n + (CH_3)_2CO \rightarrow (CH_3)_2CO\cdot Z\cdot(Et_2O)_{n-1} + Et_2O \quad (5)$$

where Z denotes the Grignard reagents, and the subscript n is 2 for the monomer and cyclic dimer, or 3 for the linear dimer. It is noted that there can be several isomeric forms for $(CH_3)_2CO\cdot Z\cdot(Et_2O)_{n-1}$, depending on the position of $(CH_3)_2CO$. Here we only considered the complexes that are directly related to the reaction products, since the energies of the complexes are rather insensitive to the positions of $(CH_3)_2CO$.

The RISM-MP2-optimized geometries for the complexes of monomer and linear dimer are shown in Figures 5a and 6a, and that of cyclic dimer is in Supporting Information. The calculated energies for the substitutions (eq 5) are summarized in Table 2. We can see that the reactions of CH_3MgCl are exothermic by 1.0, 3.4, and 0.9 kcal/mol for the monomer, linear dimer, and cyclic dimer, respectively. Without the bulk solvent, the exothermicity became smaller by about 1 kcal/mol. Note that the dynamic electron correlation was very important (i.e., the HF results overestimated the exothermicity by more than 4 kcal/mol). We also considered the substitution reaction for CH_3MgBr. The results are included in Table 2, where the reactions of monomer and linear dimer were exothermic by 1.4 and 3.3 kcal/mol in solution, respectively.

Another route for the dimer−acetone complex formation has been suggested.[36] The linear dimer−acetone complex can be produced from a monomer−acetone complex and a monomer via the following reaction:

$$CH_3MgX\cdot(Et_2O)_2 + (CH_3)_2CO\cdot CH_3MgX\cdot Et_2O \rightarrow (CH_3)_2CO\cdot(CH_3MgX)_2\cdot(Et_2O)_2 + Et_2O \quad (6)$$

Here, X is Cl or Br. This reaction is exothermic by 1.5 kcal/mol for CH_3MgCl, while it is endothermic by 1.7 kcal/mol for CH_3MgBr in Et_2O solvent. However, it is noted that the solvation free energy for linear dimer seems to be underestimated compared with that for the monomer pair (see the discussion about $\Delta\Delta\mu$ in the equilibria). In fact, without the bulk solvent the reaction (eq 6) becomes exothermic by 6.1 and 3.1 kcal/mol for CH_3MgCl and CH_3MgBr, respectively. Thus, the formation of linear dimer−acetone complex is considered to be feasible even for CH_3MgBr.

After the Grignard reagent−acetone complex is produced, the C−C bond formation reaction proceeds through the paths as shown in Figure 4. The RISM-MP2-optimized geometries of transition states (TS) and products for the reactions of monomer and linear dimer complexes are shown in Figures 5 and 6, and the energies are given in Table 3. As we can see from Table 3, the barrier height for the monomeric reaction path was 16.2 kcal/mol with the exothermicity of 25.1 kcal/mol, measured from the complex with acetone that is regarded as the reactant for this reaction step. For the linear dimeric reaction path, the TS was located above the reactant by only 9.2 kcal/mol, and the exothermicity was quite large (i.e., 49.1 kcal/mol).

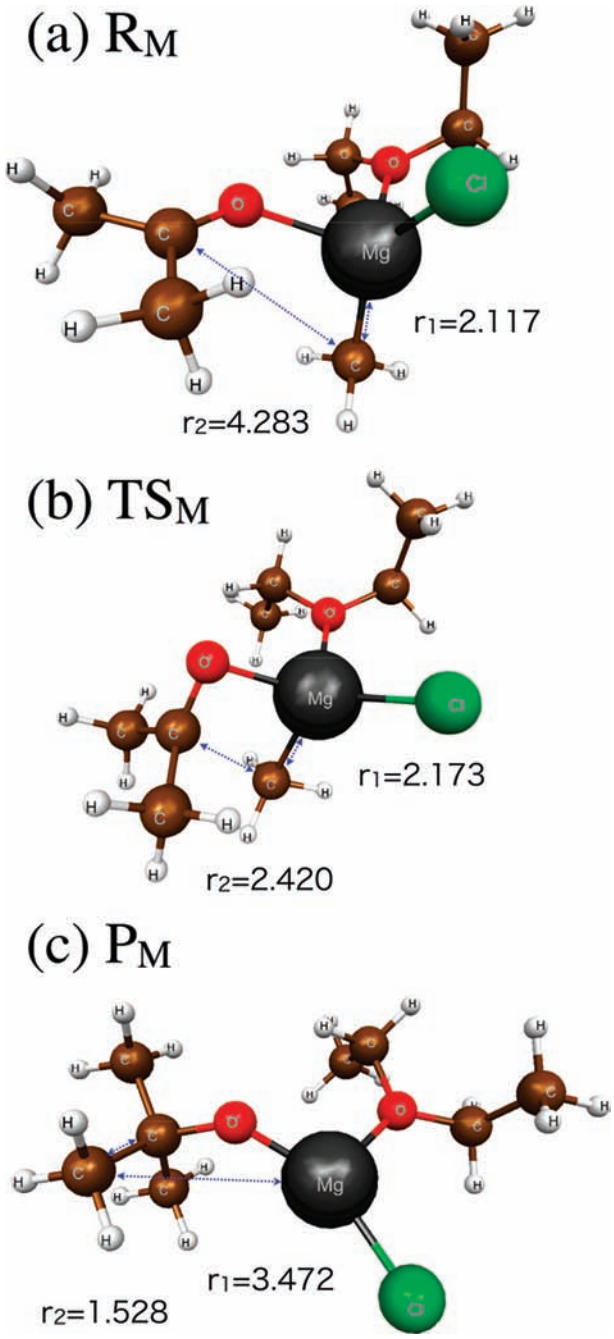

Figure 5. Geometries of (a) reactant, (b) transition state, and (c) product for the reaction of monomer with acetone. Distances are in angstroms.

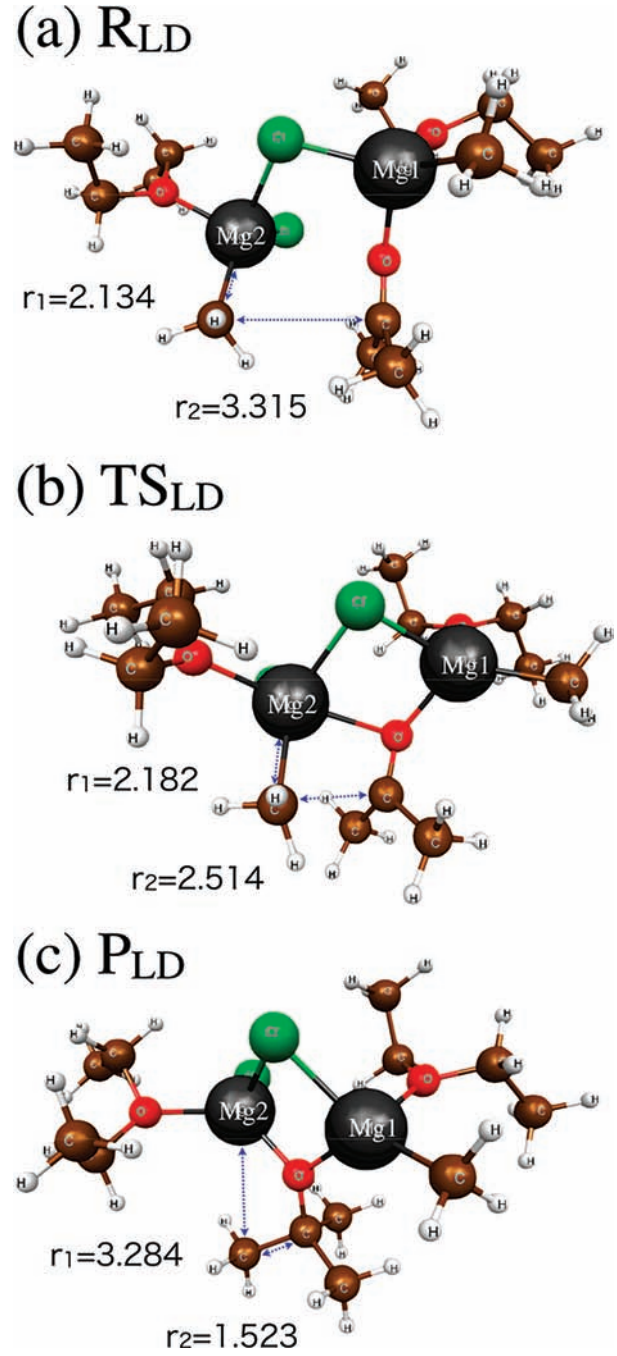

Figure 6. Geometries of (a) reactant, (b) transition state, and (c) product for the reaction of linear dimer with acetone. Distances are in angstroms.

When Br atoms were substituted for Cl, the energy barrier for monomeric and linear dimeric reaction paths became 16.7 and 9.5 kcal/mol, respectively, which are comparable with the cases of CH_3MgCl.

To see the effect of dynamic electron correlation on the energy profile for the C−C bond formation reaction, we calculated the reaction paths with the RISM-HF method. The reaction barrier heights were overestimated by 8−11 kcal/mol, and the exothermicity became small by 8−13 kcal/mol at the HF level. The electron correlation effect is also apparent on the TS geometries. The two characteristic distances, the bond-breaking Mg···C ($\equiv r_1$) and bond-forming C···C ($\equiv r_2$), are written in Figures 5 and 6. As shown in the figures, r_1 is 2.173 and 2.182 Å, and r_2 is 2.420 and 2.514 Å for the TSs of monomer (**TS_M**) and linear dimer (**TS_{LD}**), respectively. Without the electron correlation effect, r_1 of **TS_M** and **TS_{LD}** was extended to 2.251 and 2.264 Å, while r_2 was shortened to 2.299 and 2.384 Å, indicating that the geometries of TSs are shifted to the reactant side by the electron correlation. This is consistent with the Hammond postulate that the TS becomes earlier with increasing exothermicity.

TABLE 2: Energies of the Substitution Reaction (in Kilocalories per Mole)[a]

	monomer	linear dimer	cyclic dimer
CH_3MgCl	−1.0 (−0.1)	−3.4 (−2.6)	−0.9 (0.1)
CH_3MgBr	−1.4(−0.5)	−3.3 (−3.1)	−0.8 (0.2)

[a] Energies without bulk solvent are also shown in the parentheses.

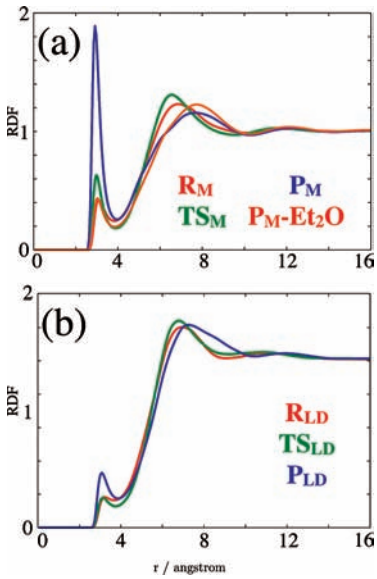

Figure 7. Radial distribution functions between Mg and O of (a) monomer and (b) linear dimer. Red, green, and blue lines are for reactant, transition state, and product, respectively. Orange line in (a) is for a complex of $\mathbf{P_M}$ with Et_2O.

TABLE 3: Energies of the Reactant, Transition State, and Product for the C−C Bond Formation Reaction of the CH_3MgCl−Acetone Complexes[a]

	monomer	linear dimer	cyclic dimer
reactant	0.0 (0.0)	0.0 (0.0)	0.0 (0.0)
transition state	16.2 (15.4)	9.2 (7.5)	15.9 (14.7)
intermediate[b]			−33.5 (−32.9)
product	−25.1 (−25.1)	−49.1 (−51.0)	−41.4 (−42.7)
product−Et_2O[c]	−43.3 (−46.6)		−55.4 (−61.0)

[a] Energy of each reactant is set to zero. Values in parentheses are energies without bulk solvent. [b] See Supporting Information and ref 6. [c] Tetrahedrally coordinated product formed by adding one more Et_2O molecule.

As seen in Figure 5, the product in the monomeric reaction path ($\mathbf{P_M}$) includes a tertiary coordinated Mg atom, since the methyl group is eliminated from the Mg along the reaction path. This implies that anther Et_2O molecule is expected to coordinate to the product $\mathbf{P_M}$. To verify this, the RDFs between the O atoms in bulk Et_2O solvent and the Mg atoms in solute are shown in Figure 7a. We can see that, while the first peak for the reactant $\mathbf{R_M}$ is very small, the peak is largely increased at the product $\mathbf{P_M}$ as in Figure 7a. Indeed, the coordination numbers at $\mathbf{R_M}$ and $\mathbf{P_M}$ were calculated to be 0.25 and 0.75, respectively. To estimate the coordination effect of additional Et_2O molecule to the product $\mathbf{P_M}$, we included one more Et_2O molecule into the QM region. As a result, the reaction exothermicity increased by 18.2 kcal/mol (given as "product−Et_2O" in Table 3). The coordination number of Et_2O to Mg thus reduced to 0.25 for the tetrahedrally coordinated product. It is noteworthy that the first peak in the linear dimeric reaction path did not change largely even at the product ($\mathbf{P_{LD}}$) because the Mg atoms are tetrahedrally coordinated throughout the reaction, as seen in Figure 6.

The RDFs at monomeric and dimeric transition states, $\mathbf{TS_M}$ and $\mathbf{TS_{LD}}$, are also given in Figure 7. For the monomeric reaction, the peak at $\mathbf{TS_M}$ was similar to that in the reactant $\mathbf{R_M}$, in contrast to the large peak in the first solvation shell of the product $\mathbf{P_M}$. The first peak for $\mathbf{TS_{LD}}$ was also very close to that for $\mathbf{R_{LD}}$. The coordination numbers in $\mathbf{TS_M}$ and $\mathbf{TS_{LD}}$ were 0.32 and 0.11, which are similar to those at $\mathbf{R_M}$ and $\mathbf{R_{LD}}$, 0.25 and 0.11. Therefore, we can conclude that the solvation structures at the TSs ($\mathbf{TS_M}$ and $\mathbf{TS_{LD}}$) are similar to those at the reactants ($\mathbf{R_M}$ and $\mathbf{R_{LD}}$), indicating that the solvation properties of TSs are well described by the present RISM-MP2 calculations. Note that, for the RDFs of linear dimer, we only plotted those of Mg2 (Figure 6), since the reaction occurs around this Mg atom and the RDF around Mg1 did not change during the reaction.

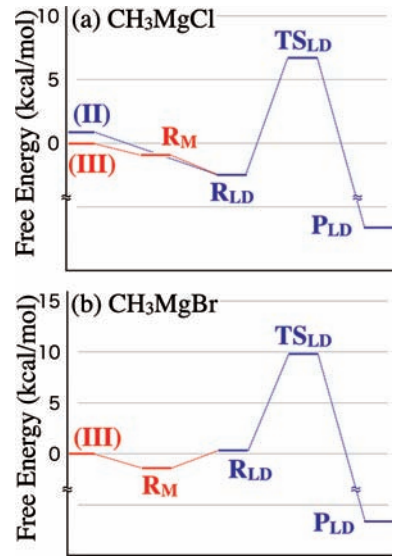

Figure 8. Proposed mechanisms for reaction of (a) CH_3MgCl and (b) CH_3MgBr with acetone in Et_2O solvent. Energies are in kilocalories per mole, and the energy of the monomer pair in the equilibria is set to zero.

We also examined the reaction of CH_3MgCl cyclic dimer with acetone, since it has been studied in Me_2O solvent.[6] The results are given in Table 3 and Supporting Information. The energy barrier in this path was 15.9 kcal/mol, which was much higher than the linear dimeric reaction path. Therefore, we can conclude that this reaction path does not contribute to the actual Grignard reaction in Et_2O solvent.

Historically, the reaction mechanism involving a six-member ring transition state has been discussed to interpret the experiments.[36−38] This reaction is considered to start from a pair of monomer−acetone complex and monomer, followed by the formation of a six-member complex between them. We first examined the complex where two Mg atoms are bridged by the methyl group instead of chloride, as proposed by Swain and Boyles.[36] The energy at the RISM-MP2-optimized geometry was higher than that of linear dimer $\mathbf{R_{LD}}$ for CH_3MgCl by 4.8 kcal/mol in Et_2O solvent, indicating that the complex involving the Mg···Cl···Mg bridge is more stable than that with the Mg···CH_3···Mg one. We next calculated a six-member transition state starting from the linear dimer complex $\mathbf{R_{LD}}$ by shortening the distance r_2 in Figure 6a. However, we could not find a six-member transition state and only the $\mathbf{TS_{LD}}$ in Figure 6b was obtained. This is because the coordination of O atom to Mg strongly stabilizes the TS energy. Indeed, the dimer products with O bridge was observed in the experiments.[39,40]

Finally, Figure 8 summarizes the reaction mechanisms of CH_3MgCl and CH_3MgBr with acetone in Et_2O solvent. Note that we only considered the dilute solution of the Grignard reagents. As mentioned above, CH_3MgCl in Et_2O is equilibrated between the monomer and linear dimer species ((III) ⇌ (II)). Therefore, as shown in Figure 8a, there are two possible paths for this reaction: (i) (II) ⇌ $\mathbf{R_{LD}}$ → $\mathbf{TS_{LD}}$ → $\mathbf{P_{LD}}$ and (ii) (III) ⇌

$\mathbf{R_M} \rightleftharpoons \mathbf{R_{LD}} \rightarrow \mathbf{TS_{LD}} \rightarrow \mathbf{P_{LD}}$. Although the monomeric reactant state ($\mathbf{R_M}$) is formed in path (ii), the C−C bond formation occurs only through $\mathbf{TS_{LD}}$ by forming $\mathbf{R_{LD}}$, since the energy of $\mathbf{TS_M}$ is located much higher than that of $\mathbf{TS_{LD}}$ (i.e., by 8.5 kcal/mol). For CH_3MgBr (in Figure 8b), the monomer state (III) is the main species in dilute solution, which is more stable than the linear dimer state (II). The reaction is expected to proceed through (III) $\rightleftharpoons$ ($\mathbf{R_M}$) $\rightleftharpoons$ ($\mathbf{R_{LD}}$) $\rightarrow$ ($\mathbf{TS_{LD}}$) $\rightarrow$ ($\mathbf{P_{LD}}$). Even for CH_3MgBr, the reaction is not likely to proceed through $\mathbf{TS_M}$, since the energy of $\mathbf{TS_M}$ is higher than $\mathbf{TS_{LD}}$ by 5.5 kcal/mol.

4. Conclusions

In this article, we studied theoretically the equilibria of the Grignard reagents CH_3MgCl and CH_3MgBr in solution and the reactions with acetone. As the solvent, we employed Et_2O, which is commonly used in organic synthesis studies. Since some of the solvent Et_2O molecules strongly coordinate to the Mg atoms, which are stable in tetrahedrally coordinated forms, we constructed cluster models explicitly involving these Et_2O molecules for all the species appearing in the equilibria and embedded them in the bulk solvent. To describe the equilibria and reactions in Et_2O solvent, the recently developed RISM-MP2 free energy gradient method was applied to optimize the geometries of species involved in the equilibria and to trace the reaction paths. The results obtained here are summarized as follows.

For the equilibria:

(1) Although the cyclic dimer structure was considered to participate in the equilibria for a long time, the linear dimer structure was found to be more stable than the cyclic dimer. This result indicates that the dimer that appears in the equilibria is of the linear form, not the cyclic one.

(2) While the monomer and linear dimer of CH_3MgCl in dilute solution coexist, the linear dimer of CH_3MgBr is more unstable than the monomer of CH_3MgBr. This is consistent with experimental findings.[1,2,13,15,17]

For the reaction:

(1) The Grignard reagent−acetone complex for the monomer and linear dimer is produced easily. Moreover, the linear dimer−acetone complex is as stable as the monomer one, even for CH_3MgBr.

(2) The barrier height for the linear dimeric reaction path is lower than the monomeric one. This indicates that the reaction proceeds through the linear dimeric path.

(3) The solvation structures at the TSs are similar to those at the Grignard reagent−acetone complex. This means that the TSs exist near the reactant states, which is consistent with the calculated large reaction exothermicity.

(4) The proposed reaction mechanism for CH_3MgCl with acetone is (i) linear dimer (II) $\rightleftharpoons \mathbf{R_{LD}} \rightarrow \mathbf{TS_{LD}} \rightarrow \mathbf{P_{LD}}$ and (ii) monomer pair (III) $\rightleftharpoons \mathbf{R_M} \rightleftharpoons \mathbf{R_{LD}} \rightarrow \mathbf{TS_{LD}} \rightarrow \mathbf{P_{LD}}$, while for CH_3MgBr, it is monomer pair (III) $\rightleftharpoons$ ($\mathbf{R_M}$) $\rightleftharpoons$ ($\mathbf{R_{LD}}$) $\rightarrow$ ($\mathbf{TS_{LD}}$) $\rightarrow$ ($\mathbf{P_{LD}}$).

It is noted that two reaction mechanisms were proposed for the alkyl group transfer in the Grignard reaction (i.e., polar and single electron transfer (SET)), depending on the type of the alkyl groups. It is recognized that the reactions occur via the polar mechanism for aliphatic ketones, while the aromatic ones prefer the SET mechanism.[1,6,17] We therefore focused on the polar mechanism for the present case.

This work has provided a new insight to the equilibria of the Grignard reagent CH_3MgX in Et_2O solvent and the reaction with acetone. However, there are still many problems to be solved for the Grignard reactions, such as the reactions of aromatic ketones or reactions in THF solvent, to fully obtain understanding of the reaction mechanism. These problems are subjects of future works, and we believe that the present study may become a guide to challenge such problems.

Acknowledgment. This work was supported by the Grant-in-Aid for Scientific Research from the Ministry of Education and Science in Japan. T.M. acknowledges the Research Fellowships of the Japan Society for the Promotion of Science for Young Scientists.

Appendix: United-Atom Model for the Solute Molecule.

Within the united-atom model, the molecule is represented by five sites (i.e., O, two CH_2, and two CH_3), though an Et_2O molecule consists of 15 atoms. To apply this united-atom model to the solute part of the RISM-SCF method, the charges of both nuclei and electrons were assigned to the sites as *effective charges*, with the least-squares fitting to reproduce the electrostatic potential.[25] The effective charges $\mathbf{q}^{\mathrm{eff}}$ are given as

$$\mathbf{q}^{\mathrm{eff}} = \mathbf{q}^{(\mathrm{N})} + \mathbf{q}^{(\mathrm{e})} \tag{A1}$$

where

$$\mathbf{q}^{(\mathrm{N})} = \tilde{\mathbf{a}}^{-1}(\mathbf{a}'\mathbf{Z} + \mathbf{c}\mathbf{Z}^{\mathrm{c(N)}}) - \frac{\tilde{\mathbf{a}}^{-1}\mathbf{1}}{\mathbf{1}^{\mathrm{t}}\tilde{\mathbf{a}}^{-1}\mathbf{1}}\{\mathbf{1}^{\mathrm{t}}\tilde{\mathbf{a}}^{-1}(\mathbf{a}'\mathbf{Z} + \mathbf{c}\mathbf{Z}^{\mathrm{c(N)}}) - N_{\mathrm{N}}\} \tag{A2}$$

$$\mathbf{q}^{(\mathrm{e})} = -\tilde{\mathbf{a}}^{-1}\{\mathrm{tr}(\mathbf{PB}) + \mathbf{c}\mathbf{Z}^{\mathrm{c(e)}}\} + \frac{\tilde{\mathbf{a}}^{-1}\mathbf{1}}{\mathbf{1}^{\mathrm{t}}\tilde{\mathbf{a}}^{-1}\mathbf{1}}[\mathbf{1}^{\mathrm{t}}\tilde{\mathbf{a}}^{-1}\{\mathrm{tr}(\mathbf{PB}) + \mathbf{c}\mathbf{Z}^{\mathrm{c(e)}}\} - \mathrm{tr}(\mathbf{PS})] \tag{A3}$$

The definitions of a′, $\mathbf{Z}$, N_{N}, $\mathbf{P}$, $\mathbf{B}$, and $\mathbf{S}$ follow those used in ref 25. $\tilde{\mathbf{a}}^{-1}$ is defined as

$$\tilde{\mathbf{a}}^{-1} \equiv \mathbf{a} - \mathbf{c} \tag{A4}$$

where $\mathbf{a}$ is also given in ref 25. $\mathbf{Z}^{\mathrm{c(N)}}$ and $\mathbf{Z}^{\mathrm{c(e)}}$ are nuclear and electronic reference charges, respectively, and $\mathbf{c}$ is the restrained electrostatic potential (RESP) constant parameter.[28]

The form of eqs A2 and A3 are similar to that of Ten-no et al.[25] However, since the charge fitting is also done for nuclear charges in eq A2, the analytic gradients of these charges with respect to nuclear coordinates are required in addition to the electronic part.[26] The gradients of the nuclear charge part can be easily evaluated by

$$\frac{\partial \mathbf{q}^{(\mathrm{N})}}{\partial \mathbf{R_a}} = \left(1 - \frac{\tilde{\mathbf{a}}^{-1}\mathbf{1}}{\mathbf{1}^{\mathrm{t}}\tilde{\mathbf{a}}^{-1}\mathbf{1}}\mathbf{1}^{\mathrm{t}}\right)\left[\frac{\partial \tilde{\mathbf{a}}^{-1}}{\partial \mathbf{R_a}}(\mathbf{a}'\mathbf{Z} + \mathbf{c}\mathbf{Z}^{\mathrm{c(N)}}) + \tilde{\mathbf{a}}^{-1}\frac{\partial \mathbf{a}'}{\partial \mathbf{R_a}}\mathbf{Z} - \frac{\partial \tilde{\mathbf{a}}^{-1}}{\partial \mathbf{R_a}}\frac{\mathbf{1}}{\mathbf{1}^{\mathrm{t}}\tilde{\mathbf{a}}^{-1}\mathbf{1}}\{\mathbf{1}^{\mathrm{t}}\tilde{\mathbf{a}}^{-1}(\mathbf{a}'\mathbf{Z} + \mathbf{c}\mathbf{Z}^{\mathrm{c(N)}}) - N_{\mathrm{N}}\}\right] \tag{A5}$$

On the other hand, the gradients of the electronic charge parts $(\partial \mathbf{q}^{(\mathrm{e})})/(\partial \mathbf{R_a})$ are almost identical to the previous result.[26] Indeed, we only have to replace "$\mathbf{a}$" and "tr($\mathbf{PB}$)" in ref 26 with "$\tilde{\mathbf{a}}$" and "tr($\mathbf{PB}$) + $\mathbf{c}\mathbf{Z}^{\mathrm{c(e)}}$" to include the RESP part.

Using these equations, we can easily apply the united-atom model to the RISM-SCF method, which enables us to apply this method to systems with many atoms efficiently.

Supporting Information Available: Potential parameters for solvent and solute molecules (Table SI1). Geometries of the reactant, transition state, intermediate, and product for the reaction of cyclic dimer with acetone (Figure SI1). This material is available free of charge via the Internet at http://pubs.acs.org.

References and Notes

(1) *Handbook of Grignard Reagents*; Silverman, G. S., Rikita, P. E., Eds.; Marcel Dekker: New York, 1996.

(2) Lindesll, W. E. In *Comprehensive Organometallic Chemistry*; Wilkinson, G., Ed.; Pergamon Press: Elmsford, NY, 1982.

(3) *Grignard Reagents: New Developments*; Richey, H. G., Jr., Ed.; Wiley: New York, 2000.

(4) Schulze, V.; Nell, P. G.; Burton, A.; Hoffmann, R. W. *J. Org. Chem.* **2003**, *68*, 4546–4548.

(5) Reetz, M. T. *Acc. Chem. Res.* **1993**, *26*, 462–468.

(6) Yamazaki, S.; Yamabe, S. *J. Org. Chem.* **2002**, *67*, 9346–9353.

(7) Ye, J.; Huang, P.; Lu, X. *J. Org. Chem.* **2007**, *72*, 35–42.

(8) Guggenberger, L. J.; Rundle, R. E. *J. Am. Chem. Soc.* **1968**, *90*, 5375–5378.

(9) Spek, A. L.; Voorbergen, P.; Schat, G.; Blomberg, C.; Bickelhaupt, F. *J. Organomet. Chem.* **1974**, *77*, 147–151.

(10) Smith, M. B.; Becker, W. E. *Tetrahedron Lett.* **1965**, *43*, 3843–3847.

(11) Smith, M. B.; Becker, W. E. *Tetrahedron* **1967**, *23*, 4215–4227.

(12) Holm, T. *Acta Chem. Scand.* **1969**, *23*, 579–586.

(13) Ashby, E. C.; Smith, M. B. *J. Am. Chem. Soc.* **1964**, *86*, 4363–4370.

(14) Smith, M. B.; Becker, W. E. *Tetrahedron* **1966**, *22*, 3027–3036.

(15) Walker, F. W.; Ashby, E. C. *J. Am. Chem. Soc.* **1968**, *91*, 3845–3850.

(16) Parris, G. E.; Ashby, E. C. *J. Am. Chem. Soc.* **1971**, *93*, 1206–1213.

(17) Ashby, E. C.; Laemmle, J.; Neumann, H. M. *Acc. Chem. Res.* **1974**, *7*, 272–280.

(18) Axten, J.; Troy, J.; Jiang, P.; Trachtman, M.; Bock, C. W. *Struct. Chem.* **1994**, *5*, 99–107.

(19) Tammiku-Taul, J.; Burk, P.; Tuulmets, A. *J. Phys. Chem. A* **2004**, *108*, 133–139.

(20) Tammiku, J.; Burk, P.; Tuulmets, A. *J. Phys. Chem. A* **2001**, *105*, 8554–8561.

(21) Ehlers, A. W.; van Klink, G. P. M.; van Eis, M. J.; Bickelhaupt, F.; Nederkoorn, P. H. J.; Lammertsma, K. *J. Mol. Model.* **2000**, *6*, 186–194.

(22) Ohkubo, K.; Watanabe, F. *Bull. Chem. Soc. Jpn.* **1971**, *44*, 2867–2868.

(23) Kato, H.; Tsuruya, S. *Bull. Chem. Soc. Jpn.* **1973**, *46*, 1001–1003.

(24) Mori, T.; Kato, S. *Chem. Phys. Lett.* **2007**, *437*, 159–163.

(25) Ten-no, S.; Hirata, F.; Kato, S. *J. Chem. Phys.* **1994**, *100*, 7443–7453.

(26) Sato, H.; Hirata, F.; Kato, S. *J. Chem. Phys.* **1996**, *105*, 1546–1551.

(27) Stevens, W. J.; Krauss, M.; Basch, H.; Jaisen, P. G. *Can. J. Chem.* **1992**, *70*, 612–630.

(28) Bayly, C. I.; Cieplak, P.; Cornell, W. D.; Kollman, P. A. *J. Phys. Chem.* **1993**, *97*, 10269–10280.

(29) Spackman, M. A. *J. Comput. Chem.* **1996**, *17*, 1–18.

(30) Briggs, J. M.; Matsui, T.; Jorgensen, W. L. *J. Comput. Chem.* **1990**, *11*, 958–971.

(31) Cornell, W. D.; Cieplak, P.; Bayly, C. I.; Gould, I. R.; Mertz, K. M., Jr.; Ferguson, D. M.; Spellmeyer, D. C.; Fox, F.; Caldwell, J. W.; Kollman, P. A. *J. Am. Chem. Soc.* **1995**, *117*, 5179–5197.

(32) Fox, T.; Kollman, P. A. *J. Phys. Chem. B* **1998**, *102*, 8070–8079.

(33) Wang, J.; Cieplak, P.; Kollman, P. A. *J. Comput. Chem.* **2000**, *21*, 1049–1074.

(34) Schmidt, M. W.; Baldridge, K. K.; Boatz, J. A.; Elbert, S. T.; Gordon, M. S.; Jensen, J. H.; Koseki, S.; Matsunaga, N.; Nguyen, K. A.; Su, S.; Windus, T. L.; Dupuis, M.; Montgomery, J. A., Jr. *J. Comput. Chem.* **1993**, *14*, 1347–1363.

(35) Ishida, T.; Hirata, F.; Kato, S. *J. Chem. Phys.* **1999**, *110*, 3938–3945.

(36) Swain, C. G.; Boyles, H. B. *J. Am. Chem. Soc.* **1951**, *73*, 870–872.

(37) Ashby, E. C.; Duke, R. B.; Newmann, H. M. *J. Am. Chem. Soc.* **1967**, *89*, 1964–1965.

(38) Ashby, E. C. *Q. Rev. Chem. Soc.* **1967**, *21*, 259–285.

(39) Bell, N. A.; Moseley, P. T.; Shearer, H. M. M. *Acta Crystallogr.* **1984**, *C40*, 602–604.

(40) Coates, G. E.; Helsop, J. A.; Redwood, M. E.; Ridley, D. *J. Chem. Soc. A* **1968**, 1118–1125.

JP9009788